Supplementary information to

Quantitative prediction of coherence times of molecular quantum bits

S. Lenz[a], K. Bader[a], H. Bamberger[a] and J. van Slageren[a,]*

Index

1. Synthesis

All reagents and solvents (including [Cu(acac)$_2$], **1**) were used as purchased from commercial sources.

1.1. [Cu(tfacac)$_2$] (2)

Copper(II) acetate monohydrate (1 mmol, 199.6 mg) was dissolved in demineralized water (10 ml) under stirring and heat (80 °C). 1,1,1-Trifluoro-2,4-pentanedione (2 mmol, 308.2 mg) in ethanol (1.7 ml) was added dropwise to the hot solution. Under vigorous stirring, sodium carbonate (0.226 mmol, 24 mg) was added and stirred for 15 min (90 °C). The resulting lavender solid was filtered, washed with 2 x 20 ml demineralized water and dried in vacuo. The crude product was recrystallized from ethanol/water (6 ml, 1:1). The final product was dried for two weeks in a desiccator over P_2O_5, resulting in a purple solid. Elemental analysis: found (calcd.) for $C_{10}H_8CuF_6O_4$ in %: C: 32.51 (32.49), H: 2.246 (2.180); UV/VIS in chloroform: λ_{max} in nm: 298, 316, 546, 678; IR (KBr-pellet): $\tilde{\nu}$ in cm^{-1}: 1611, 1587, 1531, 1518, 1478, 1417, 1367, 1312, 1226, 1196, 1168, 1139.

1.2. [Cu(hfacac)$_2$] (3)

Copper(II) acetate monohydrate (2.5 mmol, 499.1 mg) was dissolved in demineralized water (20 ml) under stirring and heat (90 °C). 1,1,1,5,5,5-Hexafluoro-2,4-pentanedione (5 mmol, 0.708 ml) and 10 ml of 4 N $NaOH_{aq}$ were added subsequently to the hot solution. After 5, a bright green solid precipitated which was filtered and washed with 2 x 10 ml demineralized water. The product was dried for two weeks in a desiccator over P_2O_5, resulting in a blue-green solid. Elemental analysis: found (calcd.) for $C_{10}H_2CuF_{12}O_4$ in %: C: 25.08 (25.12), H: 0.683 (0.420); UV/VIS in chloroform: λ_{max} in nm: 309, 328, 571, 712; IR (KBr-pellet): $\tilde{\nu}$ in cm^{-1}: 1646, 1612, 1562, 1536, 1473, 1443, 1365, 1259, 1217, 1150, 1105.

1.3. [Cu(fod)$_2$] (4)

Copper(II) acetate monohydrate (1 mmol, 200 mg) was dissolved in methanol (50 ml). This solution was added dropwise to a solution of 6,6,7,7,8,8,8-heptafluoro-2,2-dimethyl-3,5-octanedione (2 mmol, 0.47 ml) and sodium methoxide (2 mmol, 108 mg) in methanol (25 ml). The mixture was stirred at 60 °C for 30 minutes. After evaporation of the solvent, the resulting crude solid was dissolved in dichloromethane and filtered. The dichloromethane was then evaporated and blue powder of Cu(fod)$_2$ was obtained. After drying the compound in vacuo, the color changed from blue to violet. Elemental analysis: found (calcd.) for $C_{20}H_{20}CuF_{14}O_4$ in %: C: 36.76 (36.74), H: 3.27 (3.08); UV/VIS in dichloromethane: λ_{max} in nm: 244, 302, 317, 688; IR (KBr-pellet): $\tilde{\nu}$ in cm^{-1}: 2977, 2938, 2916, 2874, 1615, 1514, 1458, 1347, 1229.

1.4. [Cu(bzac)$_2$] (5)

Copper(II) acetate monohydrate (2 mmol, 400 mg) was dissolved in ethanol (40 ml). A solution of benzoylacetone (4 mmol, 650 mg) in ethanol (5 ml) was added dropwise to the copper solution. After 30 minutes of stirring the precipitate was separated by filtration and recrystallized from a 1:1 mixture of dichloromethane/n-hexane. A green cotton wool like product was obtained. Elemental analysis: found (calcd.) for $C_{20}H_{18}CuO_4$ in %: C: 62.02 (62.25), H: 4.68 (4.70); UV/VIS in dichloromethane: λ_{max} in nm: 258, 323, 552, 653; IR (KBr-pellet): $\tilde{\nu}$ in cm^{-1}: 3044, 2989, 2922, 1560, 1461, 1415, 1354, 1309, 1288, 1212.

1.5. [Cu(dbm)$_2$] (6)

Copper(II) sulfate (1 mmol, 160 mg) was dissolved in water (15 ml). A solution of dibenzoylmethane (2 mmol, 458 mg) and sodium hydroxide (2 mmol, 79 mg) in ethanol/water 15:1 was added dropwise to the copper solution. After 30 minutes of stirring the precipitate was separated by filtration, washed with water and diethyl ether and recrystallized from chloroform. A green powder was obtained. Elemental analysis: found (calcd.) for $C_{30}H_{22}CuO_4$ in %: C: 70.60 (70.65), H: 4.33 (4.35); UV/VIS in dichloromethane: λ_{max} in nm: 266, 283, 350, 555, 649; IR (KBr-pellet): $\tilde{\nu}$ in cm^{-1}: 3063, 3026, 1591, 1539, 1485, 1454, 1403, 1314, 1232.

1.6. [Pd(dbm)$_2$] (7)

Palladium(II) chloride (1 mmol, 180 mg) and sodium chloride (1.2 mmol, 70 mg) were dissolved in ethanol/water (10 ml 4:1). A solution of dibenzoylmethane (2 mmol, 460 mg) in ethanol (10 ml) was added dropwise to the palladium solution. After the addition of sodium hydroxide in water (1 mmol, 40 mg in 2 ml), a green powder precipitated which was filtrated, washed with water and diethyl ether and recrystallized from chloroform as yellow crystals. Elemental analysis: found (calcd.) for $C_{30}H_{22}O_4Pd$ in %: C: 65.16 (65.17), H: 4.09 (4.01); IR (KBr-pellet): $\tilde{\nu}$ in cm^{-1}: 1587, 1534, 1522, 1490, 1483, 1465, 1452, 1379, 1312, 1300, 1233.

2. Pulsed Q-Band EPR and HFEPR

All pulsed measurements were performed on a homebuilt Q-band EPR spectrometer, where an Oxford Instruments CF935 continuous flow cryostat (cryogenic liquid: He) was used for reaching temperatures of 7-77 K. The samples were filled in quartz tubes, degassed by three freeze-pump-thaw cycles (solutions) respectively evacuating (powders) followed by flame sealing. In all cases, electron spin echo detected EPR spectra were recorded and simulated with the Matlab toolbox "EasySpin". Relaxation measurements were performed at the most intense resonance line, marked with an asterisk in the spectra. Spin-lattice relaxation was measured by inversion recovery, phase memory times via Hahn echo; both were fitted with exponential functions (mono-, bi- or stretched exponentials).

High-frequency EPR spectra were recorded on a home-built spectrometer. Its radiation source is a 0–20 GHz signal generator (Anritsu or VDI) in combination with an amplifier–multiplier chain (VDI) to obtain the required frequencies (80–1100 GHz). It features a quasi-optical bridge (Thomas Keating, Billingshurst, UK) and induction mode detection. The detector is a QMC Instruments magnetically tuned InSb hot electron bolometer. The sample is located in an Oxford Instruments 15/17 T cryomagnet equipped with a variable temperature insert (1.5–300 K). The spectrometer control program was written in LabView. The spectra were obtained on samples in frozen solution.

1.1. Ligand Dependence of Electron Spin Relaxation

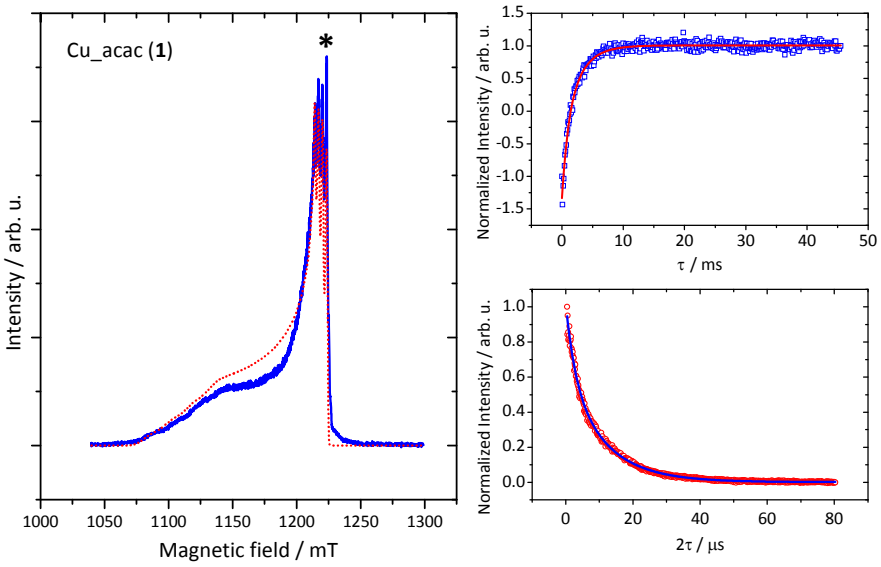

Figure S 1 Pulsed Q-band EPR spectroscopy of **1** in 0.001 M solution (1:1 CD_2Cl_2/CS_2) at 7 K. ***Left panel***: ESE detected EPR spectrum (blue, solid line) and simulation (red, broken line). Asterisk indicates field position for relaxation measurements. ***Right panel, top:*** Inversion recovery data (blue, open squares) and biexponential fit (red, solid line). ***Right panel, bottom:*** Hahn echo data (red, open circles) and biexponential fit function (blue, solid line). All simulation and fit parameters are given in Tables S 1-3.

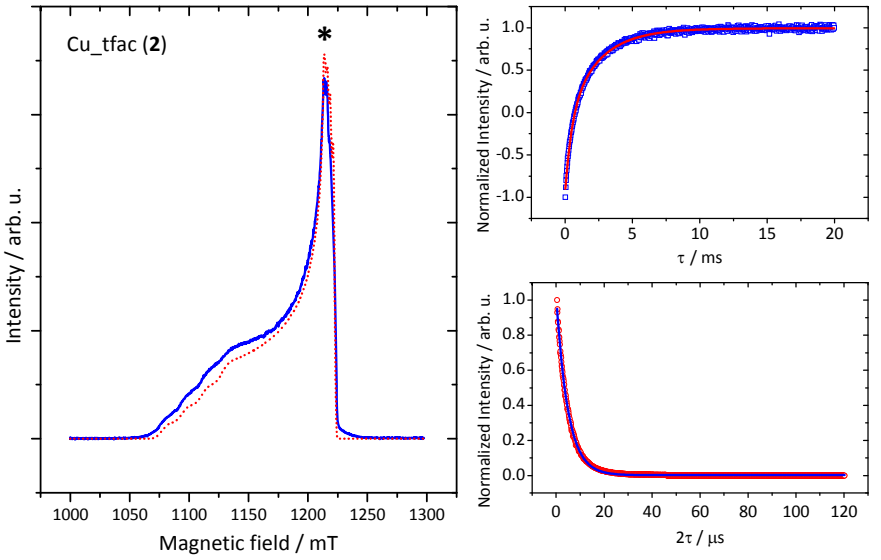

Figure S 2. Pulsed Q-band EPR spectroscopy of **2** in 0.001 M solution (1:1 CD_2Cl_2/CS_2) at 7 K. ***Left panel***: ESE detected EPR spectrum (blue, solid line) and simulation (red, broken line). Asterisk indicates field position for relaxation measurements. ***Right panel, top:*** Inversion recovery data (blue, open squares) and biexponential fit (red, solid line). ***Right panel, bottom:*** Hahn echo data (red, open circles) and monoexponential fit function (blue, solid line). All simulation and fit parameters are given in Tables S 1-3.

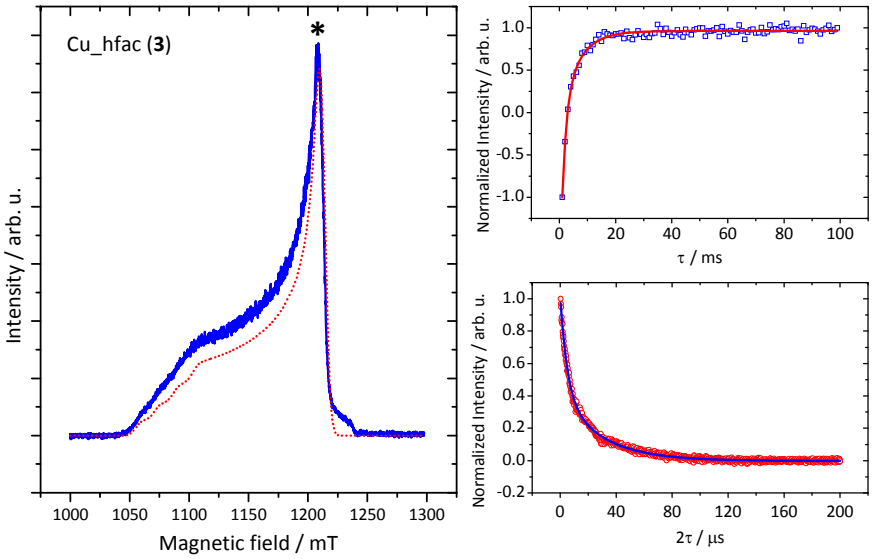

Figure S 3 Pulsed Q-band EPR spectroscopy of **3** in 0.001 M solution (1:1 CD_2Cl_2/CS_2) at 7 K. ***Left panel***: ESE detected EPR spectrum (blue, solid line) and simulation (red, broken line). Asterisk indicates field position for relaxation measurements. ***Right panel, top:*** Inversion recovery data (blue, open squares) and biexponential fit (red, solid line). ***Right panel, bottom:*** Hahn echo data (red, open circles) and biexponential fit function (blue, solid line). All simulation and fit parameters are given in Tables S 1-3.

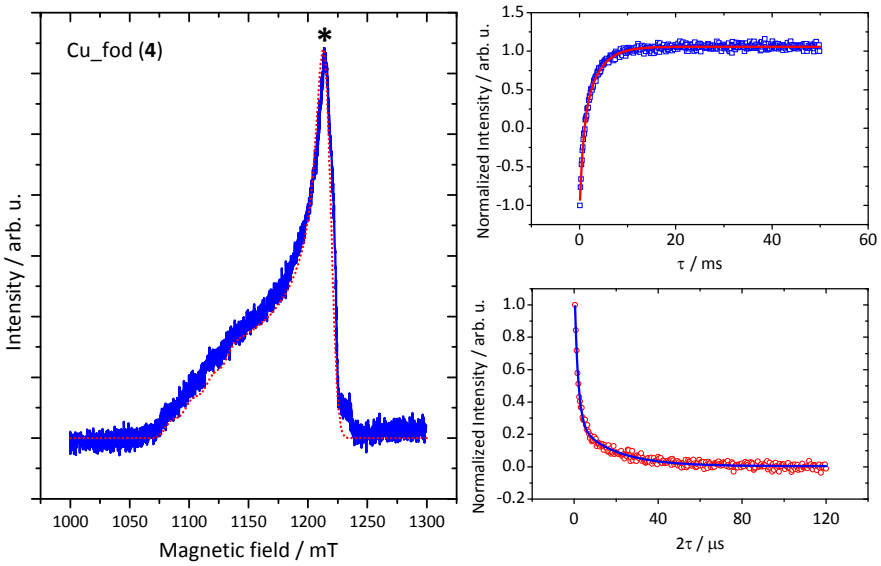

Figure S 4 Pulsed Q-band EPR spectroscopy of **4** in 0.001 M solution (1:1 CD_2Cl_2/CS_2) at 7 K. ***Left panel***: ESE detected EPR spectrum (blue, solid line) and simulation (red, broken line). Asterisk indicates field position for relaxation measurements. ***Right panel, top:*** Inversion recovery data (blue, open squares) and biexponential fit (red, solid line). ***Right panel, bottom:*** Hahn echo data (red, open circles) and biexponential fit function (blue, solid line). All simulation and fit parameters are given in Tables S 1-3.

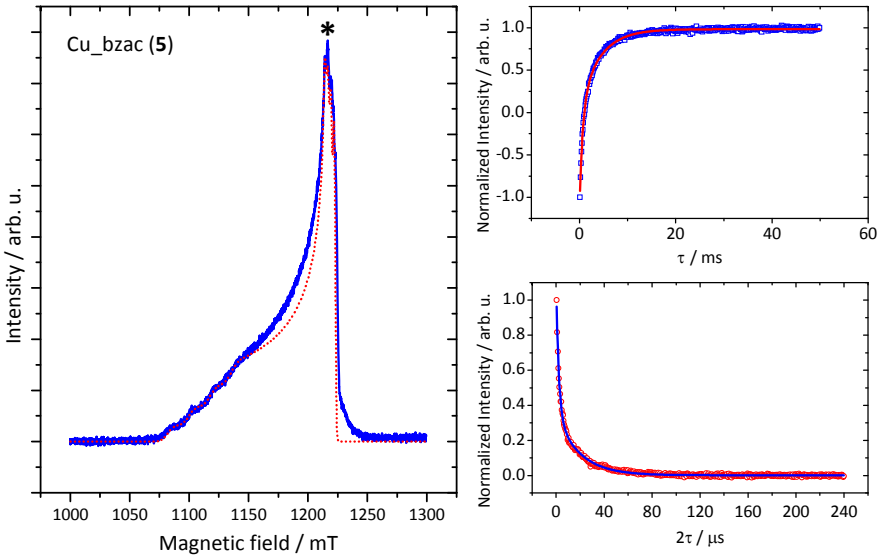

Figure S 5 Pulsed Q-band EPR spectroscopy of **5** in 0.001 M solution (1:1 CD_2Cl_2/CS_2) at 7 K. ***Left panel***: ESE detected EPR spectrum (blue, solid line) and simulation (red, broken line). Asterisk indicates field position for relaxation measurements. ***Right panel, top:*** Inversion recovery data (blue, open squares) and biexponential fit (red, solid line). ***Right panel, bottom:*** Hahn echo data (red, open circles) and biexponential fit function (blue, solid line). All simulation and fit parameters are given in Tables S 1-3.

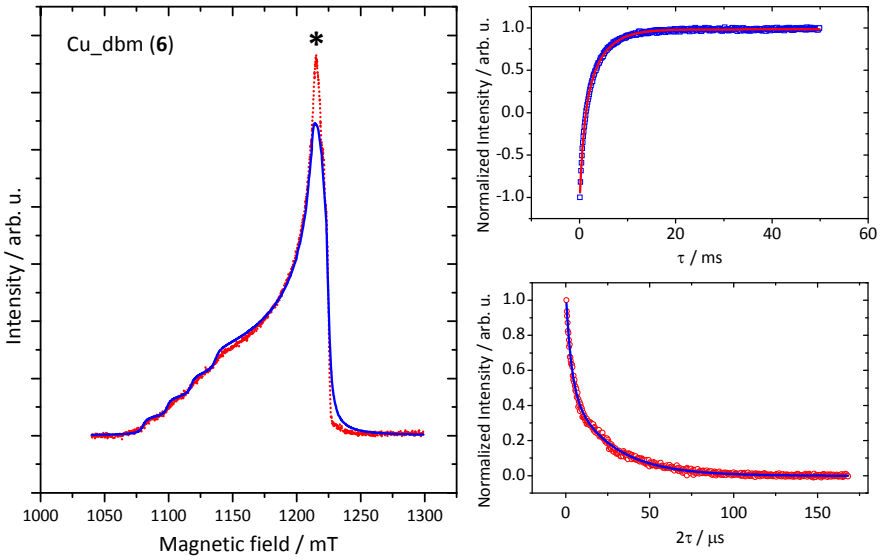

Figure S 6 Pulsed Q-band EPR spectroscopy of **6** in 0.001 M solution (1:1 CD_2Cl_2/CS_2) at 7 K. ***Left panel***: ESE detected EPR spectrum (blue, solid line) and simulation (red, broken line). Asterisk indicates field position for relaxation measurements. ***Right panel, top:*** Inversion recovery data (blue, open squares) and biexponential fit (red, solid line). ***Right panel, bottom:*** Hahn echo data (red, open circles) and biexponential fit function (blue, solid line). All simulation and fit parameters are given in Tables S 1-3.

Table S 1 Simulation parameters for ESE-detected EPR spectra of compounds **1**-**6** in 0.001 M solution (1:1 CD_2Cl_2/CS_2) at 7 K and Q-band.

sample	$g_{\|\|}$	$g_\perp$	$A_{\|\|}$ / MHz	$A_\perp$ / MHz
Cu_acac (**1**)	2.26 ± 0.01	2.040 ± 0.005	520 ± 50	85 ± 5
Cu_tfac (**2**)	2.266 ± 0.005	2.052 ± 0.001	520 ± 20	70 ± 10
Cu_hfac (**3**)	2.31 ± 0.01	2.060 ± 0.005	500 ± 20	-
Cu_fod (**4**)	2.26 ± 0.01	2.057 ± 0.005	550 ± 20	-
Cu_bzac (**5**)	2.255 ± 0.005	2.052 ± 0.003	550 ± 20	70 ± 10
Cu_dbm (**6**)	2.258 ± 0.005	2.051 ± 0.001	550 ± 20	80 ± 10

Table S 2 Parameters of biexponential fit functions for inversion recovery experiments of compounds **1**-**6** in 0.001 M solution (1:1 CD_2Cl_2/CS_2) at 7 K and Q-band.

sample	A_f	$T_{1,f}$	A_s	$T_{1,s}$
Cu_acac (**1**)	-0.8 ± 0.2	0.9 ± 0.2	-1.1 ± 0.2	2.7 ± 0.3
Cu_tfac (**2**)	-0.88 ± 0.02	0.47 ±0.002	-1.18 ± 0.02	2.30 ± 0.03
Cu_hfac (**3**)	-1.40 ± 0.03	1.17 ± 0.04	-0.61 ± 0.03	6.5 ± 0.2
Cu_fod (**4**)	-1.2 ±0.1	1.1 ± 0.1	-0.8 ± 0.1	3.8 ± 0.2
Cu_bzac (**5**)	-1.15 ± 0.02	0.7 ± 0.02	-0.91 ± 0.02	4.1 ± 0.1
Cu_dbm (**6**)	-1.02 ± 0.04	1.3 ± 0.1	-0.90 ± 0.04	4.2 ± 0.1

Table S 3 Parameters of mono- or biexponential fit functions for Hahn echo experiments of compounds **1**-**6** in 0.001 M solution (1:1 CD_2Cl_2/CS_2) at 7 K and Q-band.

sample	A_f	$T_{m,f}$	A_s	$T_{m,s}$
Cu_acac (1)	0.39 ± 0.01	2.8 ±0.1	0.63 ± 0.01	11.2 ± 0.1
Cu_tfac (2)	1.032 ± 0.001	4.75 ± 0.01	-	-
Cu_hfac (3)	0.61 ± 0.01	5.0 ±0.1	0.41 ± 0.01	29.0 ±0.4
Cu_fod (4)	0.91 ±0.02	1.7 ± 0.1	0.27 ± 0.01	18 ± 1
Cu_bzac (5)	0.74 ± 0.01	2.20 ±0.04	0.35 ± 0.01	19.3 ±0.3
Cu_dbm (6)	0.42 ± 0.01	3.6 ± 0.1	0.63 ± 0.01	23.6 ± 0.3

1.2. Solvent Dependence of Electron Spin Relaxation

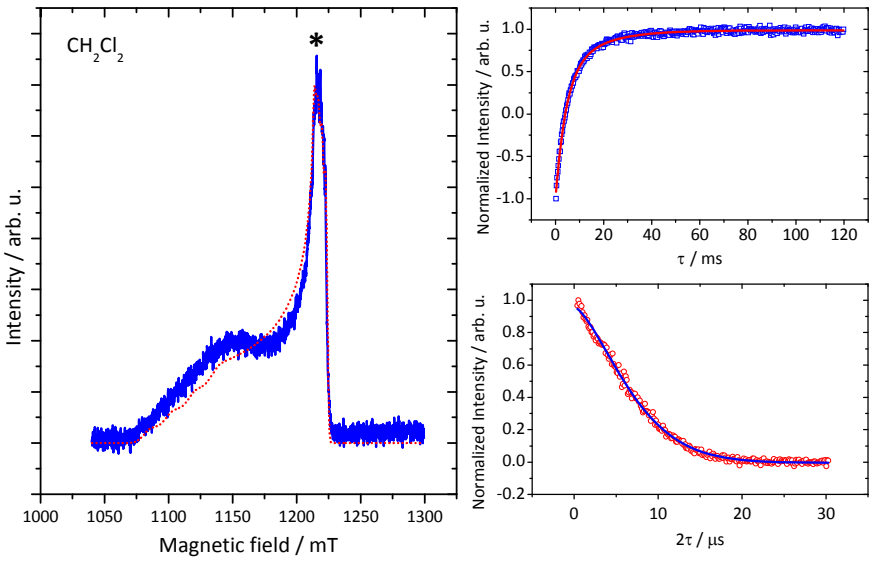

Figure S 7 Pulsed Q-band EPR spectroscopy of **6** in CH_2Cl_2-solution (0.001 M) at 7 K. ***Left panel***: ESE detected EPR spectrum (blue, solid line) and simulation (red, broken line). Asterisk indicates field position for relaxation measurements. ***Right panel, top:*** Inversion recovery data (blue, open squares) and biexponential fit (red, solid line). ***Right panel, bottom:*** Hahn echo data (red, open circles) and a stretched exponential fit according to equation 3 in the main text (blue, solid line). All simulation and fit parameters are given in Tables S 4-7.

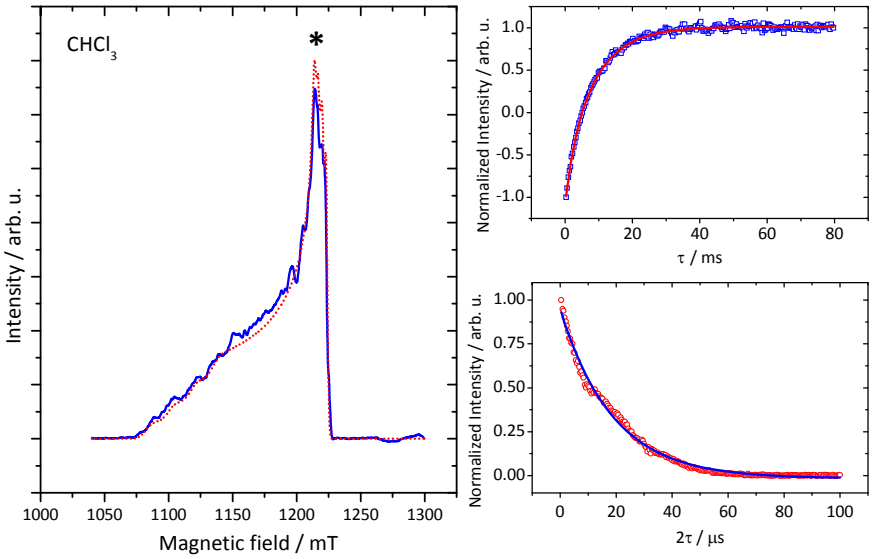

Figure S 8 Pulsed Q-band EPR spectroscopy of **6** in $CHCl_3$-solution (0.001 M) at 7 K. ***Left panel***: ESE detected EPR spectrum (blue, solid line) and simulation (red, broken line). Asterisk indicates field position for relaxation measurements. ***Right panel, top:*** Inversion recovery data (blue, open squares) and biexponential fit (red, solid line). ***Right panel, bottom:*** Hahn echo data (red, open circles) and monoexponential fit function (blue, solid line). All simulation and fit parameters are given in Tables S 4-7.

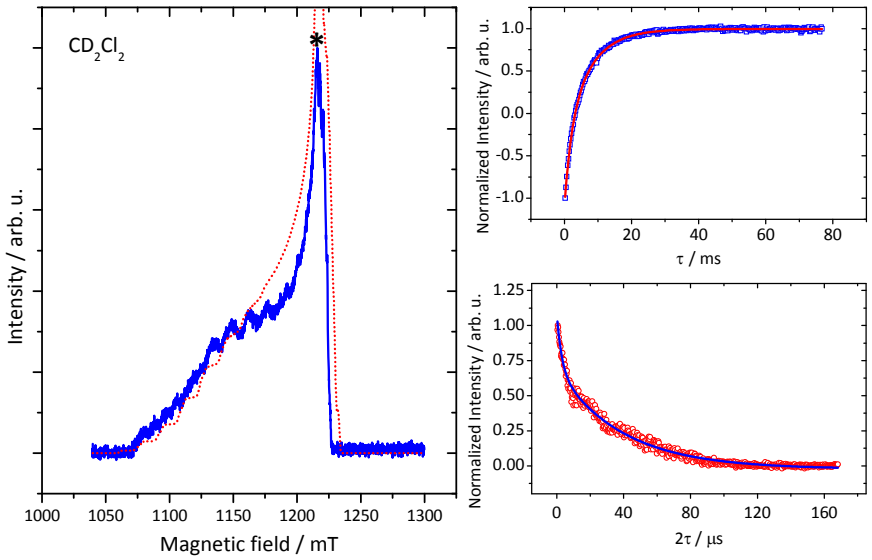

Figure S 9 Pulsed Q-band EPR spectroscopy of **6** in CD_2Cl_2-solution (0.001 M) at 7 K. ***Left panel***: ESE detected EPR spectrum (blue, solid line) and simulation (red, broken line). Asterisk indicates field position for relaxation measurements. ***Right panel, top:*** Inversion recovery data (blue, open squares) and biexponential fit (red, solid line). ***Right panel, bottom:*** Hahn echo data (red, open circles) and biexponential fit function (blue, solid line).All simulation and fit parameters are given in Tables S 4-7.

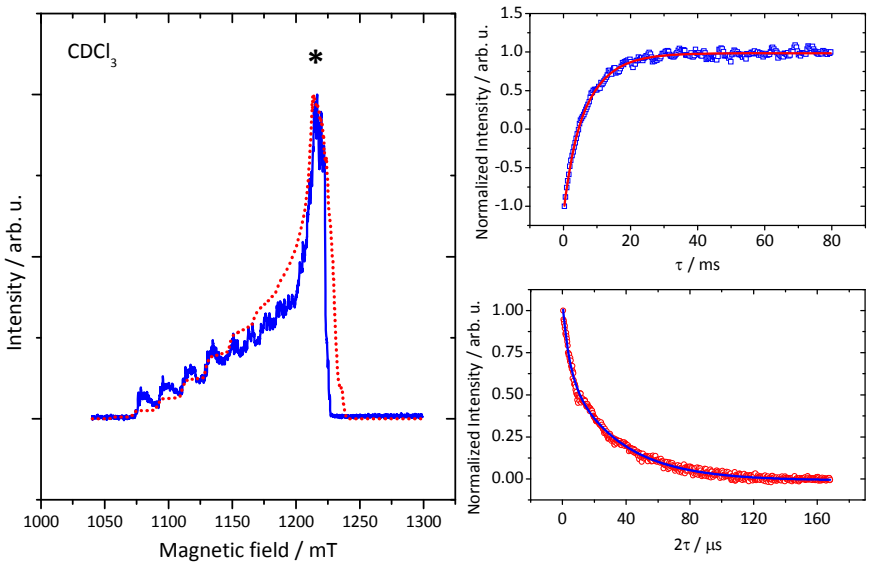

Figure S 10 Pulsed Q-band EPR spectroscopy of **6** in $CDCl_3$-solution (0.001 M) at 7 K. ***Left panel***: ESE detected EPR spectrum (blue, solid line) and simulation (red, broken line). Asterisk indicates field position for relaxation measurements. ***Right panel, top:*** Inversion recovery data (blue, open squares) and biexponential fit (red, solid line). ***Right panel, bottom:*** Hahn echo data (red, open circles) and biexponential fit function (blue, solid line).All simulation and fit parameters are given in Tables S 4-7.

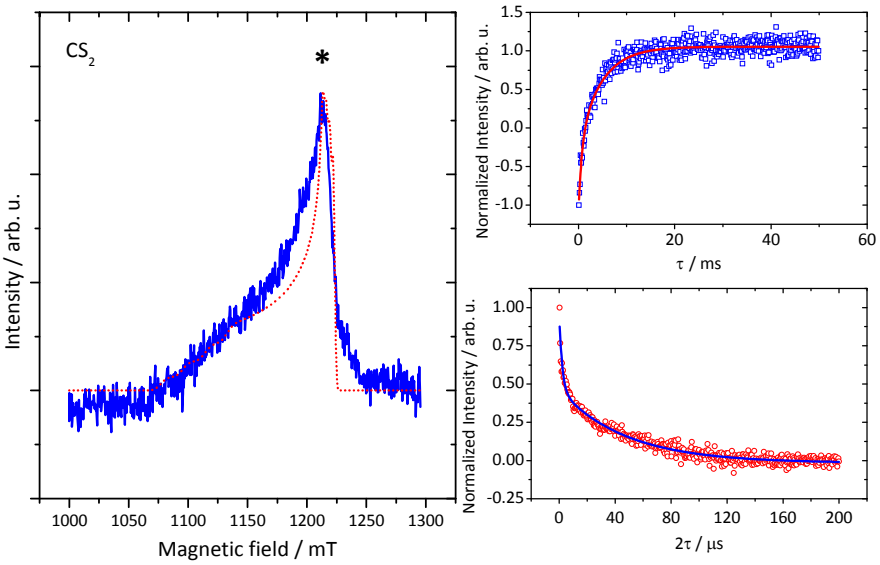

Figure S 11 Pulsed Q-band EPR spectroscopy of **6** in CS_2-solution (0.001 M) at 7 K. ***Left panel***: ESE detected EPR spectrum (blue, solid line) and simulation (red, broken line). Asterisk indicates field position for relaxation measurements. ***Right panel, top:*** Inversion recovery data (blue, open squares) and biexponential fit (red, solid line). ***Right panel, bottom:*** Hahn echo data (red, open circles) and biexponential fit function (blue, solid line).All simulation and fit parameters are given in Tables S 4-7.

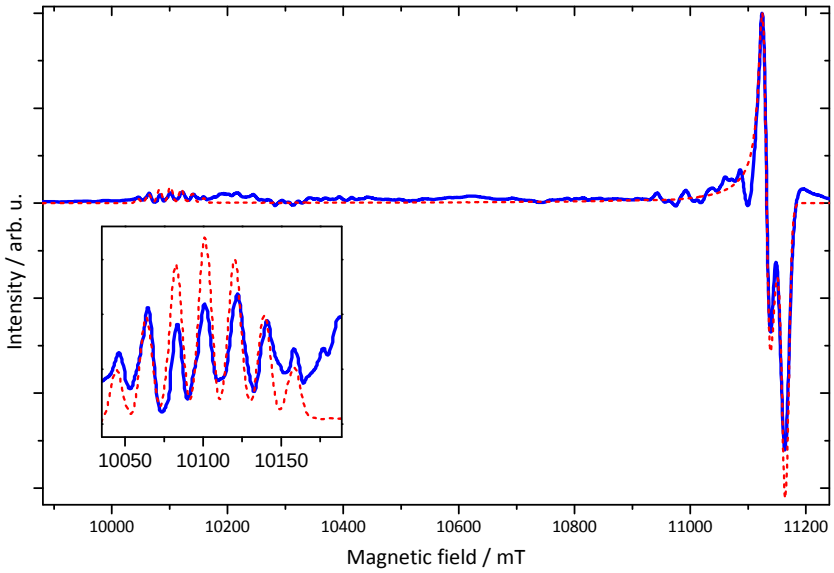

Figure S 12 HFEPR spectrum (blue, solid line) of **6** in $CDCl_3$-solution (0.001 M) at 7 K and simulation (red, broken line). All simulation parameters are given in Tables S 4-7.

Table S 4 Simulation parameters for ESE-detected EPR spectra of **6** in 0.001 M solution of various solvents at 7 K and Q-band.

solvent system	$g_{\|\|}$	$g^{\perp}$	$A_{\|\|}$ / MHz	$A^{\perp}$ / MHz
CH_2Cl_2, $CHCl_3$, CS_2	2.258 ± 0.005	2.051 ± 0.001	550 ± 20	80 ± 10

Table S 5 Simulation parameters for the EPR spectra of **6** in 0.001 M solution of $CDCl_3$ and CD_2Cl_2 at 7 K in Q-band and HFEPR. A coupled spin system of two spins with S = ½ was assumed. The dipolar coupling tensor was tilted 30° towards the x-y-plane. Each electron spin was coupled to two nuclei with the given A_{zz}.

Method and Solvent	J_{ex} / cm^{-1}	J_{dip} / MHz	g_{zz}	g_{xx}	g_{yy}	A_{zz} / MHz
HFEPR in $CDCl_3$	> 0.1 (FM)	300	2.265 ± 0.001	2.047 ± 0.001	2.053 ± 0.001	600 ± 30
Pulsed Q-Band in $CDCl_3$	> 0.1 (FM)	300	2.230 ± 0.005	2.047 ± 0.005	2.053 ± 0.005	600 ± 30
Pulsed Q-Band in CD_2Cl_2	> 0.1 (FM)	280	2.380 ± 0.005	2.047 ± 0.001	2.053 ± 0.005	520 ± 30

Table S 6 Parameters of biexponential fit functions for inversion recovery experiments of **6** in 0.001 M solution of various solvents at 7 K and Q-band.

solvent	A_f	$T_{1,f}$ / ms	A_s	$T_{1,s}$ / ms
CH_2Cl_2	-1.4 ± 0.1	4.3 ± 0.2	-0.6 ± 0.1	15 ± 1
$CHCl_3$	-0.3 ± 0.1	2.2 ± 0.5	-1.7 ± 0.1	8.7 ± 0.2
CD_2Cl_2	-1.2 ± 0.2	2.1 ± 0.8	-0.7 ± 0.2	9 ±1
$CDCl_3$	-0.4 ± 0.1	2.1 ± 0.8	-1.7 ± 0.1	7.5 ± 0.4
CS_2	-0.8 ± 0.1	0.70 ± 0.02	-1.3 ± 0.1	4.7 ± 0.3

Table S 7 Parameters of mono-/ stretched-/ biexponential fit functions for Hahn echo experiments of **6** in 0.001 M solution of various solvents at 7 K and Q-band.

solvent	A_1	$T_{M,f}$ / µs	A_2	$T_{M,s}$ / µs	k_2
CH_2Cl_2	--	--	0.962 ± 0.007	7.94 ± 0.06	1.50 ± 0.02
$CHCl_3$	--	--	0.968 ± 0.006	18.7 ± 0.2	--
CD_2Cl_2	0.40 ± 0.02	3.0 ± 0.2	0.711 ± 0.007	39.0 ± 0.7	--
$CDCl_3$	0.395 ± 0.009	4.2 ± 0.2	0.665 ± 0.007	33.6 ± 0.5	--

CS_2	0.50 ± 0.03	2.1 ± 0.2	0.481 ± 0.007	47 ± 2	--

1.3. Temperature Dependence of Electron Spin Relaxation in Solution

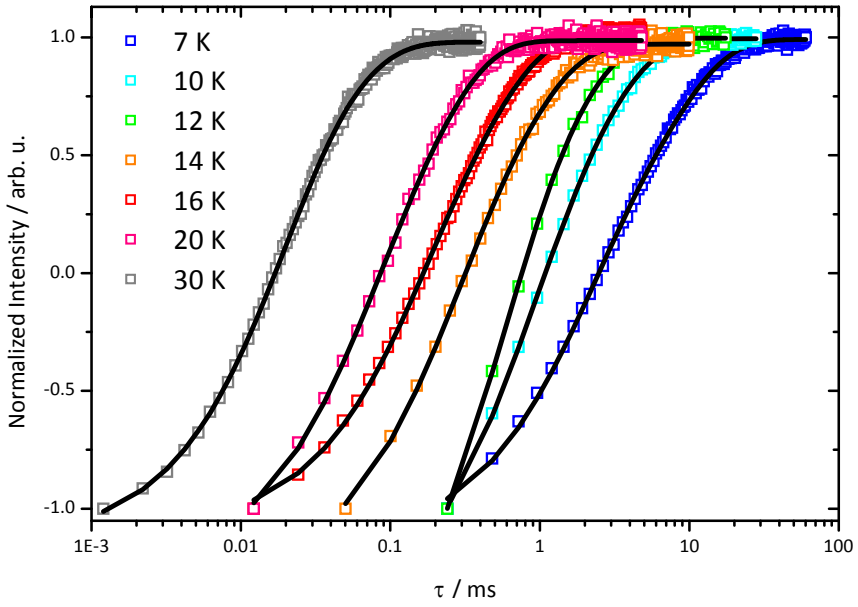

Figure S 13 Inversion recovery data (open squares) and mono-/biexponential fits (black, solid lines) of **6** in 0.001 M CD_2Cl_2/CS_2-solution (1:1) Q-band, 7-30 K. Fit parameters are given in Table S 7.

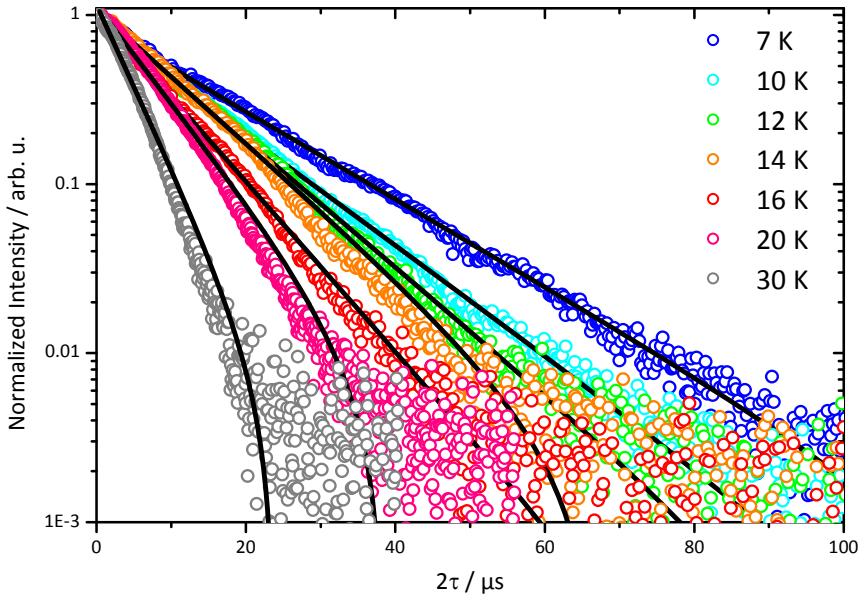

Figure S 14 Hahn echo data (open circles) and bi-/monoexponential fit functions (black, solid lines) of **6** in 0.001 M CD_2Cl_2/CS_2-solution (1:1) Q-band, 7-30 K. Fit parameters are given in Table S 8.

Table S 8 Parameters of bi-/monoexponential fit functions for inversion recovery experiments of **6** in 0.001 M CD_2Cl_2/CS_2-solution (1:1) Q-band, 7-30 K.

T / K	A_f	$T_{1,f}$ / ms	A_s	$T_{1,s}$ / ms
7	-1.02 ± 0.04	1.3 ± 0.1	-0.90 ± 0.04	4.2 ± 0.1
10	-1.21 ± 0.06	0.62 ± 0.04	-1.30 ± 0.07	2.13 ± 0.06

12	-1.6 ± 0.2	0.42 ± 0.07	-1.3 ± 0.3	1.3 ± 0.1
14	-1.0 ± 0.1	0.19 ± 0.02	-1.2 ± 0.1	0.69 ± 0.03
16	-0.87 ± 0.03	0.112 ± 0.005	-1.23 ± 0.04	0.403 ± 0.007
20	-0.87 ± 0.08	0.05 ± 0.006	-1.3 ± 0.1	0.171 ± 0.006
30	-1.2 ± 0.1	0.0154 ± 0.0008	-0.8 ± 0.1	0.04 ± 0.002

Table S 9 Parameters of bi-/monoexponential fit functions for inversion recovery- and Hahn echo experiments of **6** in 0.001 M CD_2Cl_2/CS_2-solution (1:1) Q-band, 7-30 K.

T / K	A_f	$T_{M,f}$/ µs	A_s	$T_{M,s}$ / µs
7	0.42 ± 0.01	3.6 ± 0.1	0.63 ± 0.01	23.6 ± 0.3
10	-	-	13.37 ± 0.07	13.37 ± 0.07
12	-	-	11.58 ± 0.02	11.58 ± 0.02
14	-	-	11.03 ± 0.04	11.03 ± 0.04
16	-	-	8.66 ± 0.02	8.66 ± 0.02
20	-	-	7.59 ± 0.04	7.59 ± 0.04
30	-	-	4.52 ± 0.03	4.52 ± 0.03

1.4. Electron Spin Relaxation in Doped Powder

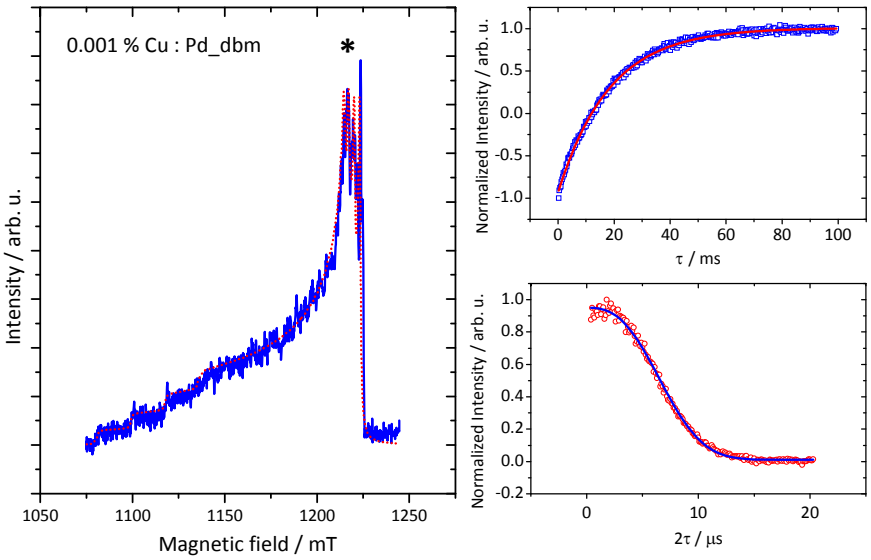

Figure S 15 Pulsed Q-band EPR spectroscopy of 0.001 % **6** in **7** ("doped powder") at 7 K. ***Left panel***: ESE detected EPR spectrum (blue, solid line) and simulation (red, broken line). Simulation parameters: $g_{||}$ = 2.255 ± 0.005, $g_{\perp}$ = 2.050 ± 0.001, $A_{||}$ = (570 ± 10) MHz, $A_{\perp}$ = (78 ± 10) MHz. Asterisk indicates field position for relaxation measurements. ***Right panel, top:*** Inversion recovery data (blue, open squares) and monoxponential fit (red, solid line). ***Right panel, bottom:*** Hahn echo data (red, open circles) and stretched exponential fit (blue, solid line). All fit parameters are given in Table S 9.

1.5. Temperature Dependence of Electron Spin Relaxation in Doped Powder

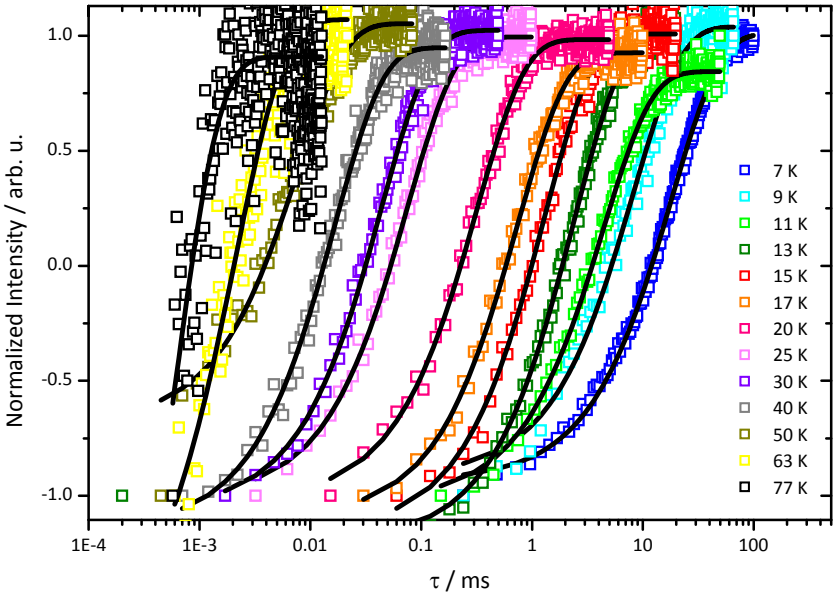

Figure S 16 Inversion recovery data (open squares) and mono-/biexponential fits (black, solid lines) of 0.001 % **6** in **7** ("doped powder) at Q-band, 7-77 K. Fit parameters are given in Table S 9.

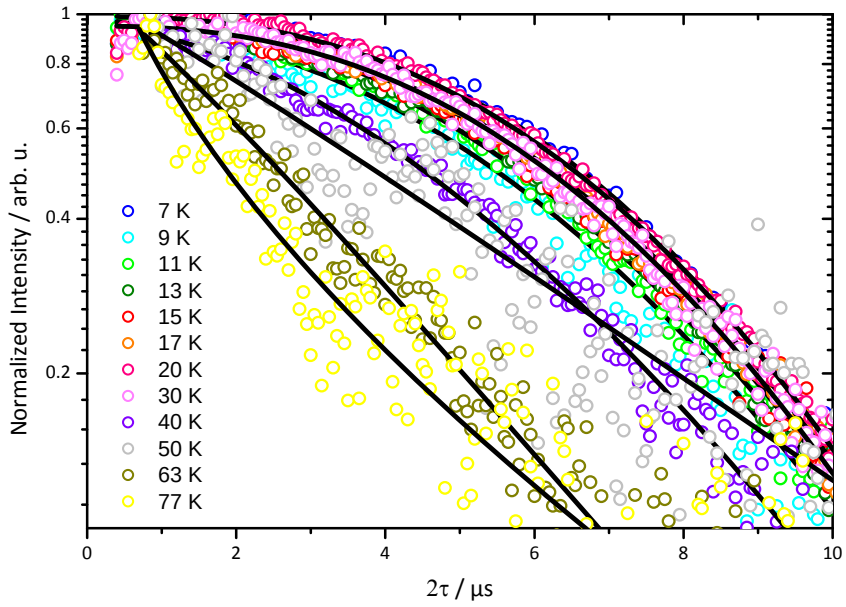

Figure S 17 Hahn echo data (open circles) and stretched exponential fits (black, solid lines) of 0.001 % **6** in **7** ("doped powder") at Q-band, 7-77 K. Fit parameters are given in Table S 9.

Table S 10 Parameters of mono- and stretched exponential fit functions for inversion recovery and Hahn echo experiments of 0.001 % **6** in **7** ("doped powder) at Q-band, 7-77 K.

T / K	T_1 / ms	T_M / µs	k
7	18.4 ± 0.1	7.74 ± 0.03	2.68 ± 0.04
9	8.2 ± 0.2	6.81 ± 0.04	2.04 ± 0.04
11	4.63 ± 0.07	7 ± 0.02	2.1 ± 0.02
13	2.4 ± 0.02	7.26 ± 0.02	2.27 ± 0.02
15	1.39 ± 0.02	7.38 ± 0.03	2.3 ± 0.03
17	0.78 ± 0.01	7.4 ± 0.02	2.3 ± 0.02
20	0.327 ± 0.004	7.54 ± 0.02	2.43 ± 0.02
30	0.077 ± 0.001	7.34 ± 0.03	2.36 ± 0.03
40	0.0456 ± 0.0007	5.78 ± 0.04	1.7 ± 0.03
50	0.0172 ± 0.0003	4.5 ± 0.3	0.9 ± 0.1
63	0.0083 ± 0.0002	3.45 ± 0.07	1.31 ± 0.05
77	0.0023 ± 0.0001	1.2 ± 0.3	0.61 ± 0.07

3. Mass Spectrometry

The measurements were recorded on a MAT 95 from *Finnigan* (70 eV) for direct insertion EI and a micrOTOFq from *Bruker Daltonics* for ESI mass spectrometry.

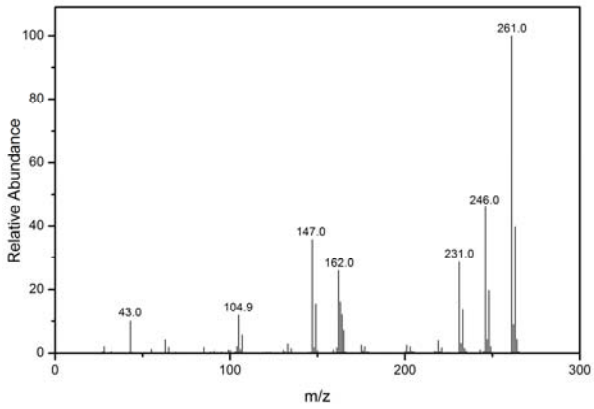

Figure S 18 Full EI Mass spectrum of **1**

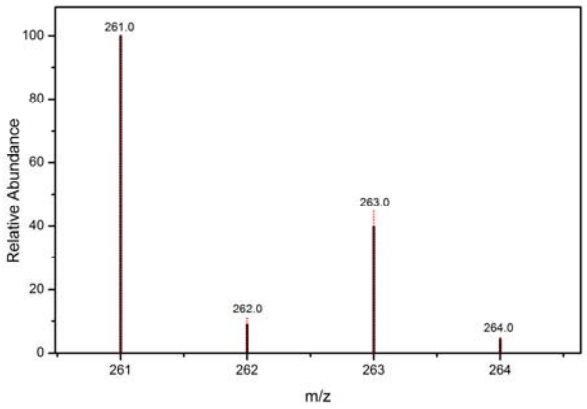

Figure S 19 EI Mass spectrum of **1** (black lines) with the corresponding simulation (red dotted lines) of $C_{10}H_{14}CuO_4$

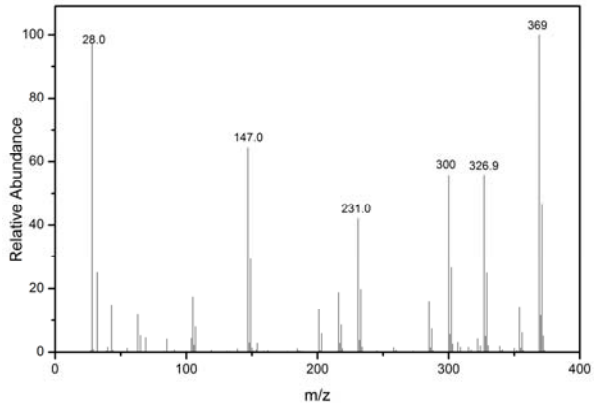

Figure S 20 Full EI Mass spectrum of **2**

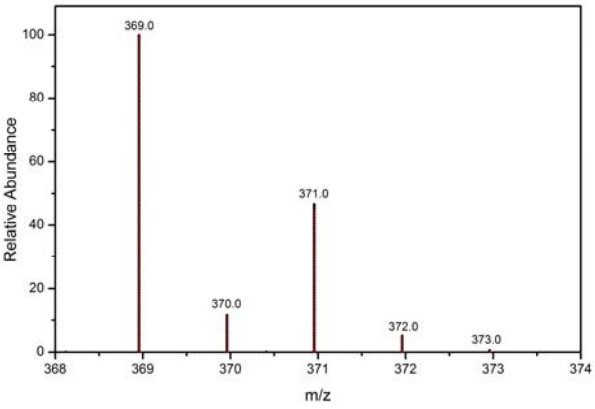

Figure S 21 EI Mass spectrum of **2** (black lines) with the corresponding simulation (red dotted lines) of $C_{10}H_8CuF_6O_4$

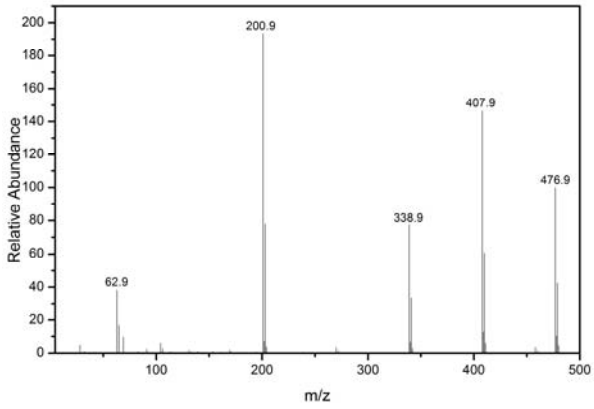

Figure S 22 Full EI Mass spectrum of **3**

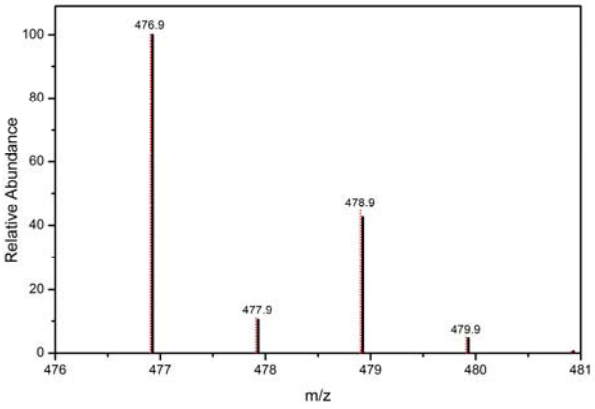

Figure S 23 EI Mass spectrum of **3** (black lines) with the corresponding simulation (red dotted lines) of $C_{10}H_2CuF_{12}O_4$

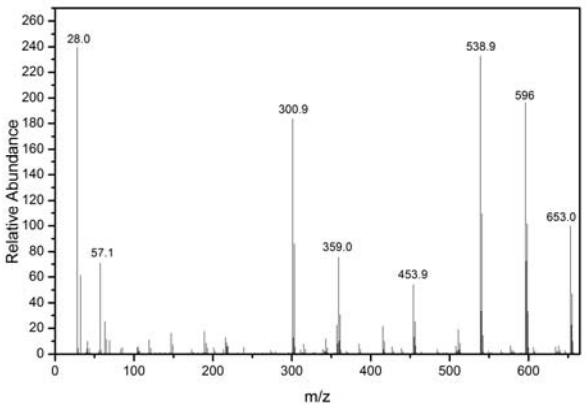

Figure S 24 Full EI Mass spectrum of **4**

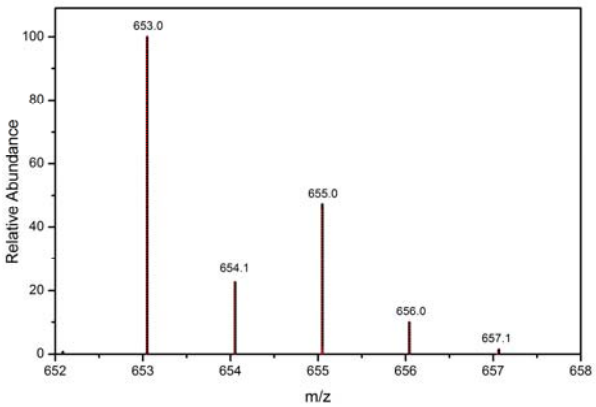

Figure S 25 EI Mass spectrum of **5** (black lines) with the corresponding simulation (red dotted lines) of $C_{20}H_{20}CuF_{14}O_4$

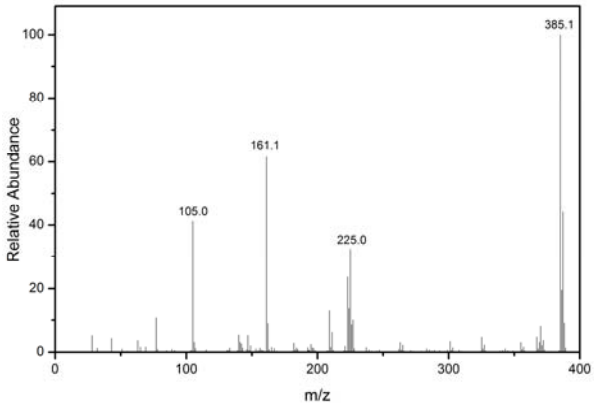

Figure S 26 Full EI Mass spectrum of **5**

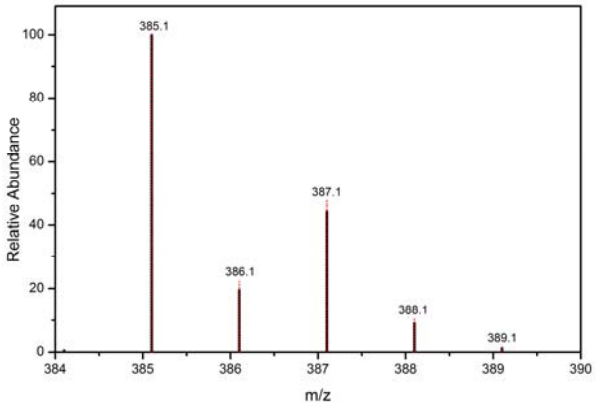

Figure S 27 EI Mass spectrum of **5** (black lines) with the corresponding simulation (red dotted lines) of $C_{20}H_{18}CuO_4$

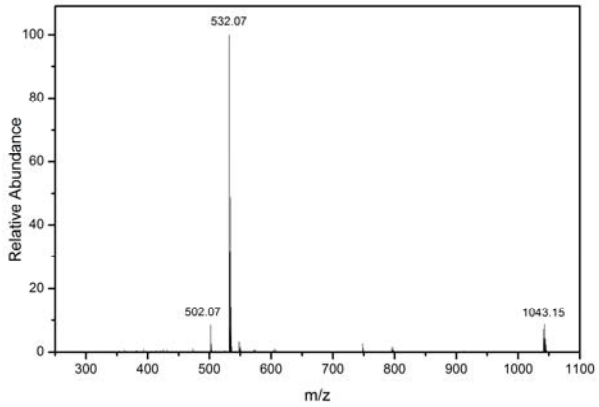

Figure S 28 Full ESI Mass spectrum of **6**

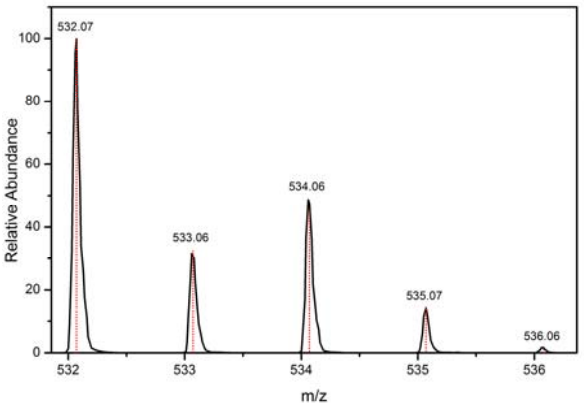

Figure S 29 ESI Mass spectrum of **6** (black lines) with the corresponding simulation (red dotted lines) of $C_{30}H_{22}CuO_4Na$

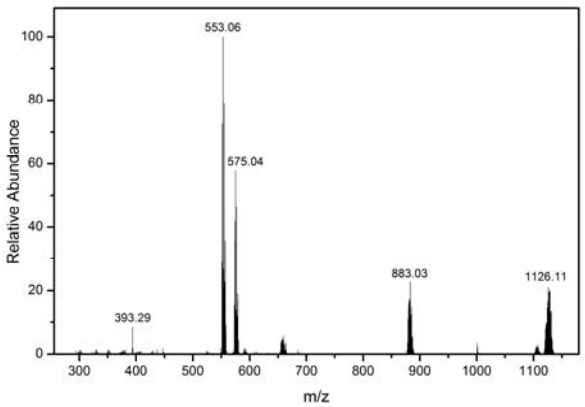

Figure S 30 Full ESI Mass spectrum of **7**

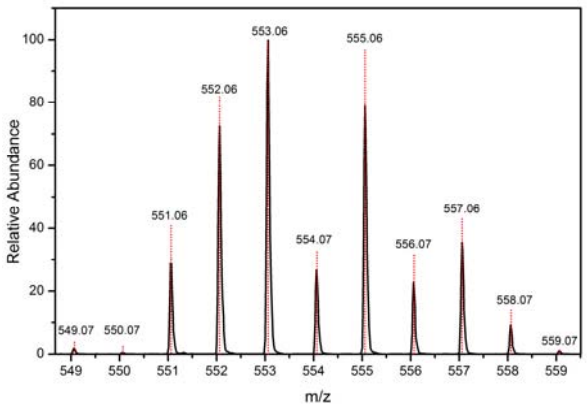

Figure S 31 ESI Mass spectrum of **7** (black lines) with the corresponding simulation (red dotted lines) of $C_{30}H_{22}PdO_4H$

Table S 11 Assignment of the fragments occurring in the mass spectra of the investigated compounds

Compound	m/z	Assignment
1 $Cu(acac)_2$	246.0	$[M\text{-}CH_3]^+$
	231.0	$[M\text{-}(CH_3)_2]^+$
	163.0	$[MH\text{-}(acac)]^+$
	162.0	$[M\text{-}(acac)]^+$
	147.0	$[M\text{-}(acac)\text{-}(CH_3)]^+$
2 $Cu(tfac)_2$	300.0	$[M\text{-}CF_3]^+$
	231.0	$[M\text{-}(CF_3)_2]^+$
	147.0	$[M\text{-}(tfac)\text{-}(CF_3)]^+$
3 $Cu(hfac)_2$	407.9	$[M\text{-}CF_3]^+$
	338.9	$[M\text{-}(CF_3)_2]^+$
	200.9	$[M\text{-}(CF_3)_2]^+$
4 $Cu(fod)_2$	596.0	$[M\text{-}C_4H_9]^+$
	538.9	$[M\text{-}(C_4H_9)_2]^+$
	359.0	$[MH\text{-}(fod)]^+$
	300.9	$[M\text{-}(fod)\text{-}C_4H_9]^+$
5 $Cu(bzac)_2$	225.0	$[MH\text{-}(bzac)]^+$
	224.0	$[M\text{-}(bzac)]^+$
	161.1	$[bzac]^+$
7 $Pd(dbm)_2$	575.05	$[MNa]^+$
	658.95	$[MPd\text{-}H]^+$
	883.04	$[M_2\text{-}(dbm)]^+$
	1126.12	$[M_2Na]^+$

4. Powder X-Ray diffraction

The measurements were performed at room temperature by Dr. Ingo Hartenbach at the Institute of Inorganic Chemistry at the University of Stuttgart using a STADI P diffractometer from *STOE* with Mo Kα1 radiation (50 kV, 40 mA), equipped with a Siemens ID 3003 generator, a Germanium (111) monochromator and a position sensitive detector. The diffractometer was operated utilizing WinXPOW software, which was also used for baseline corrections and the calculations of the theoretical powder patterns.

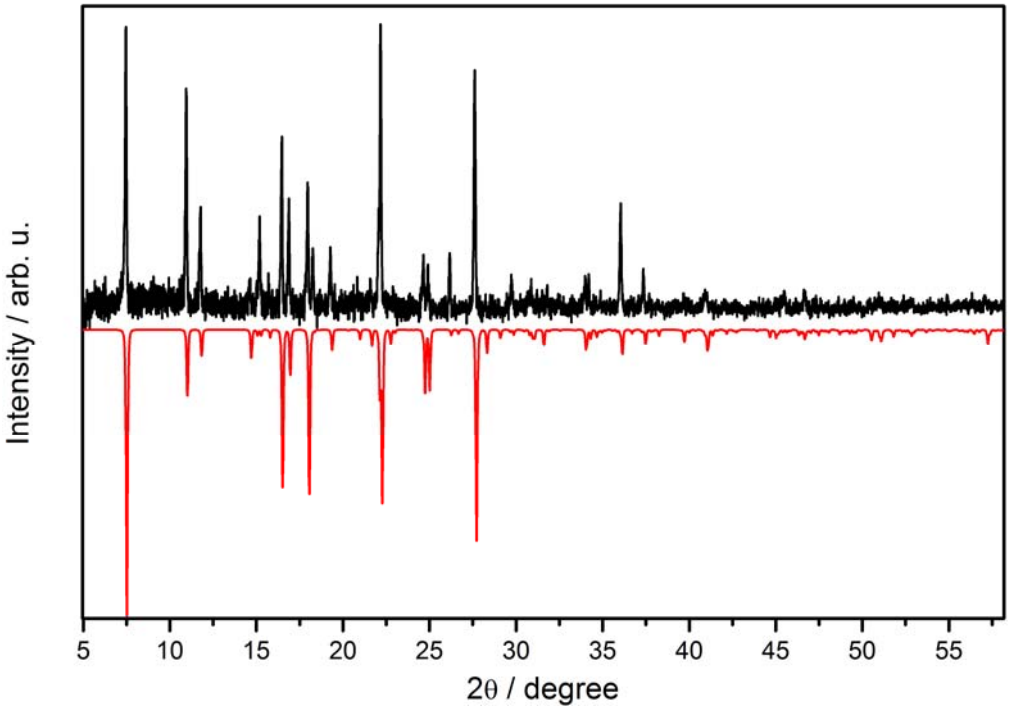

Figure S 32 Experimental powder XRD pattern of **6** and the calculated pattern based on the crystal structure from

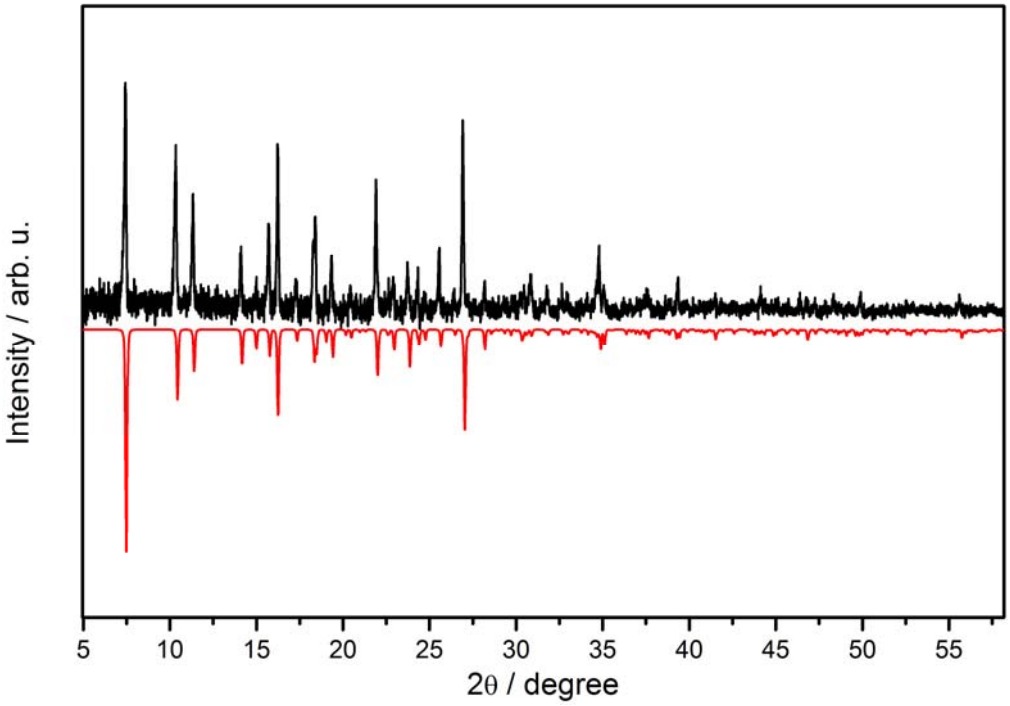

Figure S 33 Experimental powder XRD pattern of **7** and the calculated pattern based on the crystal structure from

5. Calculation of the Hahn-Echo decay

Several interactions are of relevance to calculating the echo decay. First of all, the hyperfine interaction between electron and nuclear spins:

$$\mathcal{H}^A = \sum_n A_n (I_n \cdot S) \qquad \text{(eq. 1)}$$

The hyperfine coupling constant A_n can include hyperfine and dipolar interactions. Here we assume that the Zeeman interaction is much stronger than the hyperfine interaction so that eq. 1 becomes:

$$\mathcal{H}^A \approx \sum_n A_n I_{nz} S_{nz} \qquad \text{(eq. 2)}$$

The second important interaction is the interaction between nuclear spins, which is assumed to be dipolar:

$$\mathcal{H}^B = \sum_{n \neq m} \mathcal{H}^B_{nm} \qquad \text{(eq. 3)}$$

$$\mathcal{H}^B_{nm} = \frac{\gamma_n \gamma_m \hbar}{2} \left[\frac{I_n \cdot I_m}{R^3_{nm}} - \frac{3(I_n \cdot R_{nm})(I_m \cdot R_{nm})}{R^5_{nm}} \right] \qquad \text{(eq. 4)}$$

Because the Zeeman interaction is again dominant, eq. 4 simplifies to:

$$\mathcal{H}^B_{nm} = b_{nm} (I_{n+} I_{m-} - 2 I_{nz} I_{mz}) \qquad \text{(eq. 5)}$$

$$b_{nm} = -\frac{1}{4} \gamma_n \gamma_m \hbar \frac{1 - 3\cos^2(\theta_{nm})}{R^3_{nm}} \qquad \text{(eq. 6)}$$

Here θ_{nm} is the angle between the magnetic field and the vector $\boldsymbol{R_{nm}}$ joining two nuclear spins *n* and *m*.

The Hahn-echo intensity at a specific pulse delay time τ is proportional to the expectation value of the in-plane magnetization $\langle S_x \rangle(\tau) + i \langle S_y \rangle$ at that delay time. To calculate this expectation value, Witzel et al. employ the density matrix formalism to describe the system consisting of one central electron spin and surrounding nuclear spins and propagate the density matrix in time using time propagators.{Witzel, 2006 #18655}{Schweiger, 2001 #6682} For realistic experimental conditions (B_0 > 0.1 Tesla, T > 100 mK), they arrive at the master equation:

$$v_E(\tau) = \frac{1}{M} \mathrm{Tr} \{ U_- U_+ U_-^\dagger U_+^\dagger \} \qquad \text{(eq. 7)}$$

This equation describes the intensity $v_E(\tau)$ of the Hahn-echo. Here *M* is the partition function of the nuclear spins (approx. 2^N where *N* is the number of nuclei). *U*± are the propagation operators defined as:

$$U_\pm = e^{-i \mathcal{H}^\pm \tau} \qquad \text{(eq. 8)}$$

Here the Hamilton operator $\mathcal{H}^\pm$ is defined as:

$$\mathcal{H}^\pm = \sum_{n \neq m} \mathcal{H}^B_{nm} \pm \frac{1}{2} \sum_n A_n I_{nz} \qquad \text{(eq. 9)}$$

For the systems under study, the electron spin is localized on the central metal ion and therefore we have assumed the hyperfine interaction to be dipolar in nature, leading to the following expression for the coupling constant:

$$A_n = -\gamma_n \gamma_{ES} \hbar \frac{1-3\cos^2(\theta_n)}{R_n^3} \quad \text{(eq. 10)}$$

with R_n the distance between electron and nuclear spins and θ_n the angle between $\boldsymbol{R}_n$ and the magnetic field.

Although the master equation (eq. 7) correctly treats the spin decoherence caused by nuclear spin flip-flops, it is impractical for real calculations. The reason for this is the dimension of the state space, which quickly grows with the number of nuclear spins included in the calculation. For example, already one molecule of $Cu(dbm)_2$ contains 22 protons. The corresponding dimension of the state space is 2^{22} and therefore $H^{\pm}$ is described by a $2^{22} \times 2^{22}$ matrix.

Witzel et al. provide a solution where all possible interactions are decomposed into clusters of different numbers of nuclear spins, where in the following only clusters consisting of two members (pairs) are considered, which was shown to be sufficient.{Witzel, 2006 #18655} These contributions are then combined to give the full echo intensity. The derivation by Witzel leads to the following equation for combining the pair contributions v_{nm}:

$$v_E^{(2)}(\tau) = \exp\left(\sum_{n>m} 1 - v_{nm}(\tau)\right) \quad \text{(eq. 11)}$$

For the example of one molecule $Cu(dbm)_2$ this means, that instead of single $2^{22} \times 2^{22}$ matrix, $\frac{22^2-22}{2}$ $2^2 \times 2^2$ matrices have to be calculated. In a solid, the electron spin will also feel the fluctuations due to the field of the spins of the neighbouring ions. Due to the dilute nature of the sample $\mathbf{7}_{\mathbf{0.001\%}}$ only the nuclear spins of the neighbouring atoms need to be taken into account.

For nuclear spins with $I = 1/2$ an analytical solution for the pair contributions exists:

$$v_{nm}(\tau) = 1 - \frac{c_{nm}^2}{\left(1+c_{nm}^2\right)^2}\left[\cos(w_{nm}\tau) - 1\right]^2 \quad \text{(eq. 12)}$$

$$c_{nm} = \frac{A_n - A_m}{4b_{nm}} \quad \text{(eq. 13)}$$

$$w_{nm} = 2b_{nm}\sqrt{1 + c_{nm}^2} \quad \text{(eq. 14)}$$

We have employed the following strategy for the simulation of the echo decay: From the central metal ion, we have considered contributions from all the protons within a sphere with a given radius. We have then increased the radius of the sphere until the simulation of the echo decay no longer changed. It turned out, that a radius of about 30 Å is sufficient.

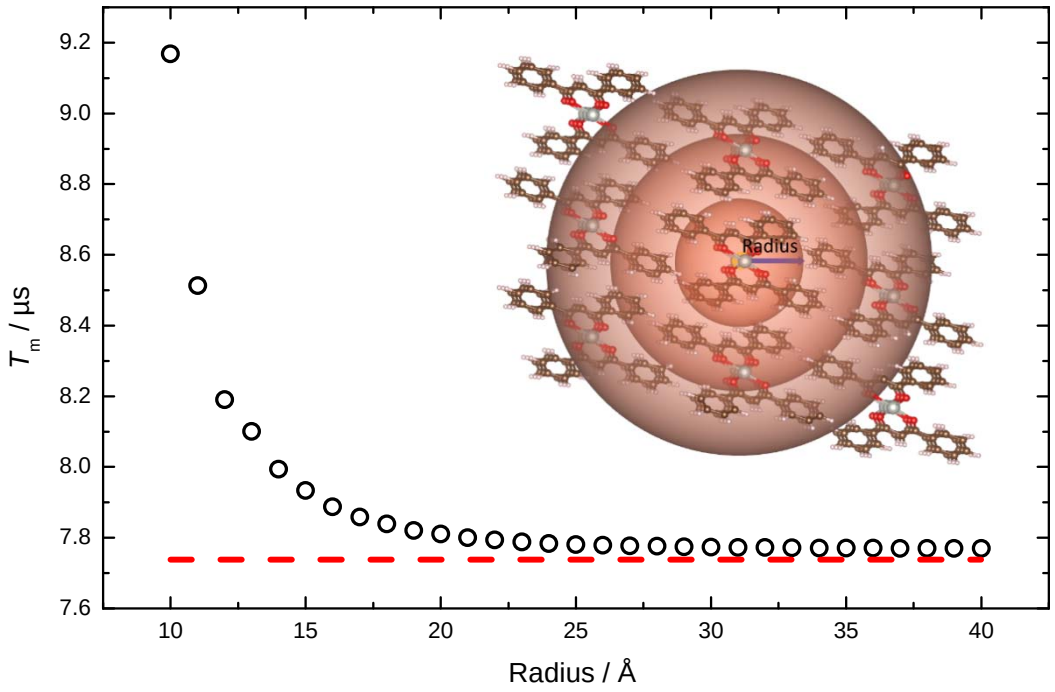

Figure S 34 Simulations of 0.001 % **6** in **7** were carried out using the method described above with an increasing radius of the sphere, which contains the considered nuclei. The resulting Hahn-echo decays were fitted with a stretched exponential to extract T_M (closed black circles). The experimental T_M of 0.001 % **6** in **7** ("doped powder") at Q-band and 7 K is also shown (red dotted line).